ORNL/SPR-2021/2225

Transverse Rupture Strength of Uranium Dioxide

Nuclear Technology Research and Development

Approved for public release.
Distribution is unlimited.

Prepared for
US Department of Energy
Advanced Fuels Campaign
A. Lupercio, C. Doyle, R. Winters,
A. Nelson and B. Jaques
Oak Ridge National Laboratory
September 17, 2021
M3FT-21OR0202010712

SUMMARY

The Advanced Fuels Campaign is currently focusing on development of accident-tolerant fuels that possess a range of property modifications intended to improve fuel performance during accident and transient conditions as well as extend license limits to burnups beyond 62 MWd/kgU. Both drivers have identified understanding and mitigating fuel cracking as a key performance criterion. Exploration of small scale mechanical testing methods for application to irradiated fuel materials has shown promise, but also emphasized the limited data regarding fracture behavior of UO_2 and doped variants in the literature. A biaxial flexure strength test was developed to be used for unirradiated UO_2. Previous work benchmarked this method against the existing literature for common oxide ceramics. This report describes initial data collected for UO_2 using this system. Fracture strength measurements made here were found to agree with the limited literature, providing confidence in its use for lesser-studied doped UO_2 and other systems.

This page is intentionally left blank.

CONTENTS

This page is intentionally left blank.

FIGURES

TABLES

This page is intentionally left blank.

ACRONYMS

AFC	Advanced Fuels Campaign
ASTM	American Society for Testing of Materials
ATF	Accident-tolerant fuel
BSE	Backscatter electron
EDS	Energy-dispersion spectroscopy
FIB	focused ion beam
ICP-MS	Inductively coupled plasma–mass spectrometry
LWR	light water reactor
MRF	Materials Research Furnaces, Inc.
MTS	Materials Test System
NIST	National Institute of Standards and Technology
ORNL	Oak Ridge National Laboratory
PCI	pellet-cladding interaction
SEM	scanning electron microscopy/microscope
TRS	Transverse rupture strength
UO_2	uranium dioxide
WPPM	weight parts per million
XRD	X-ray diffraction

This page is intentionally left blank.

FRACTURE STRENGTH DETERMINATION METHODS FOR CERAMIC MATERIALS APPLIED TO URANIUM DIOXIDE

1. INTRODUCTION

Uranium dioxide (UO_2) fuel is used as fuel in light water reactors (LWRs). While the fuel pellet is technically the first engineering barrier for radionuclide release, pellet fracturing at intermediate- to high-burnup values releases fission gases into the fuel rod plenum [1, 2]. Therefore, the true engineering barrier is the fuel cladding, which performs very well in LWR environments [3]. The extreme temperature gradients generated by fission energy and the low thermal conductivity of UO_2 quickly induce radial cracking in UO_2 during operation [4]. Cracks in the fuel provide opportunities for fuel relocation, increased fission gas release, and pellet-cladding mechanical interaction (PCMI) [5]. The ability to predict and engineer the fracture of UO_2 fuel pellets using modern computational tools is therefore a key engineering goal that has been the focus of ongoing experimental and computational efforts [6, 7]. Accurate predictions of fuel pellet cracking during operation requires knowledge of more complex phenomena, but improved understanding of the fundamental fracture behavior of unirradiated UO_2 is first necessary.

The Advanced Fuels Campaign (AFC) is currently focusing on development of accident-tolerant fuels (ATF) that possess a range of property modifications intended to improve fuel performance during accident and transient conditions. In addition, efforts are under way to understand the phenomena that limit performance at high burnups in an effort to extend license limits to burnups beyond 62 MWd/kgU. Both of these drivers have identified understanding and mitigating fuel cracking as a key criterion. A previous AFC report provided an overview of the current mechanical property database for UO_2 and evaluated the potential for small-scale test methods to address the challenge that reference materials face for examination of irradiated fuel systems [8]. This work found that data for pure UO_2 collected using cantilever beam testing was in reasonable agreement with that found in the literature and would provide a plausible means to measure the evolution of fracture behavior of grain boundaries or other features following irradiation. Subsequent efforts established biaxial flexure strength testing as a means by which to test fracture of UO_2 ceramics in a conventional manner [9]. Biaxial flexure strength testing is a conventional method for fracture determination and provides transverse rupture strength (TRS) and Weibull statistics for brittle materials according to accepted standard testing methods. This method has been benchmarked against literature data for common engineering ceramics, and been shown capable of reproducing accepted values [10].

This report describes progress made in FY 2021 in this area and presents new results obtained for pure UO_2. Synthesis of new doped UO_2 samples is also described. Dopants refer to secondary cations added to UO_2 at levels below a few weight percent with the desired impact of engineering grain size or other properties to improve performance. AFC has been investigating the synthesis, impacts to microstructure, and performance of doped UO_2 for several years. While the impacts of different dopants, dopant levels, and sintering temperature on UO_2 density and microstructure are relatively straightforward to analyze, measurement of dopant impacts on mechanical properties are more challenging to assess. The present report is focused on measurement of pure UO_2 samples, but the ability to fabricate doped samples of geometries suitable to TRS testing will provide important data elucidating the impact that dopants and microstructural variations in UO_2 have on fracture properties.

2. TRANSVERSE RUPTURE STRENGTH METHOD

An overview of the TRS method and benchmarking has been provided previously [9, 10]. Samples were loaded into the TRS test fixture as seen in the schematic representation in Figure 1 and the images in Figure 2; the samples were centered using three set screws (at 120° angles) around the circumference of the right cylindrical pellet prior to placing the punch alignment fixture on the base. The entire assembly was loaded into a metal enclosure with a lid and placed in the Materials Test System (MTS) test frame. The metal enclosure is used to contain any UO_2 particles that may be generated during the fracture process. All samples were loaded at a rate of 0.5 $^{mm}/_{min}$ while collecting force and displacement data at a sampling rate of 4 Hz using a MTS [11]. All tests were performed at room temperature and atmosphere.

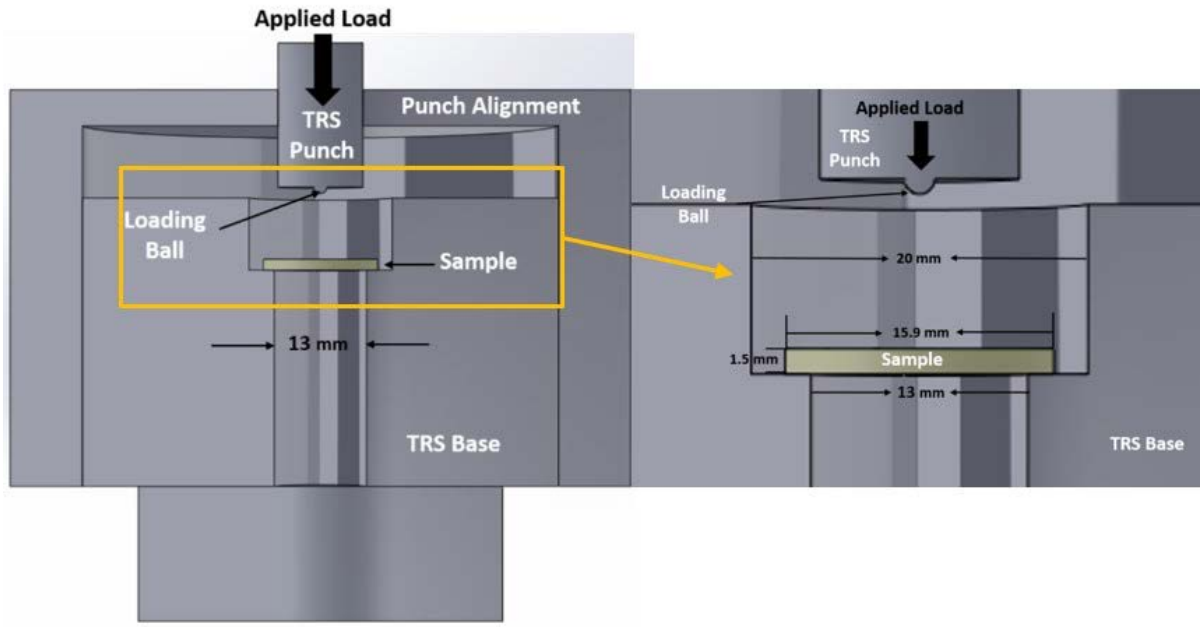

Figure 1. Cross section schematic of TRS test fixture for right cylindrical samples.

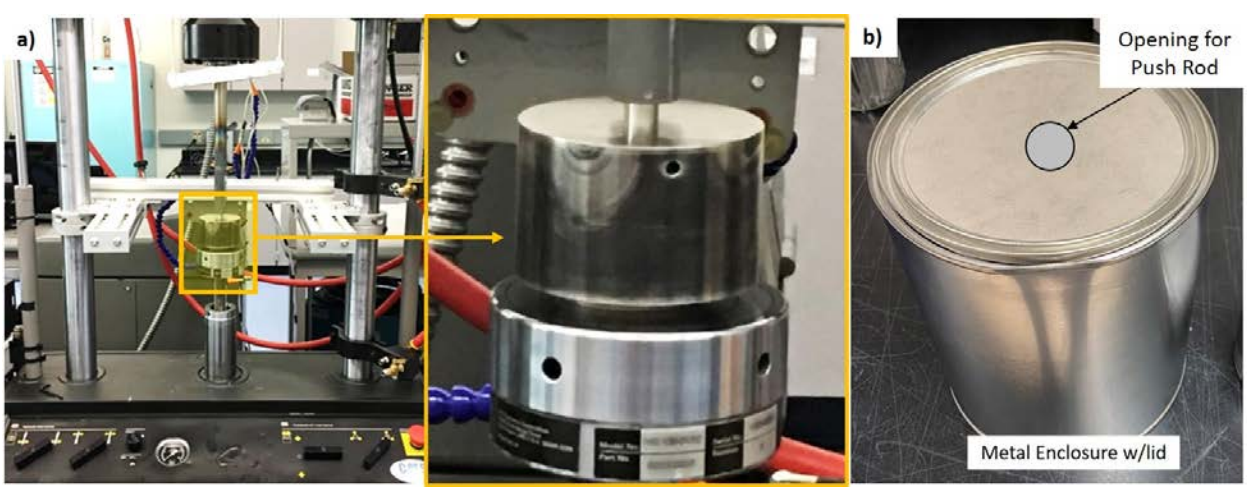

Figure 2. Images of a) TRS fixture with MTS set up and b) metal enclosure with a lid to contain possible UO_2 dust particles generated during the fracture event.

The generated data was collected and used to calculate the transverse stress to create a plot of the transverse stress vs displacement. The transverse stress (MPa) was calculated using Equation 1 [12-14].

$$\sigma = \frac{A*F}{t^2} \tag{1}$$

where t is the specimen thickness in mm, F is the applied force in Newtons, and A is a dimensionless factor that depends on the geometry of the specimen and loading ball, the ring diameter, and the Poisson's ratio of the loading ball (0.21) and test materials. The factor A is calculated using Equation 2 below.

$$A = \frac{3}{4*\pi}\left[\left(2(1+\nu_S) + ln\frac{a}{b}\right) + \frac{(1-\nu_S)(2a^2-b^2)}{2R^2} + (1+\nu_S)\right] \tag{2}$$

where ν_S is the Poisson's ratio of the test material, a is the radius of the support ring (mm), R is the radius of the test specimen (mm), and b is the contact radius of the loading ball (mm). The contact radius of the loading ball is calculated using Equation 3.

$$b = \frac{t}{3} \tag{3}$$

where t is the thickness of the test specimen (mm).

The equation used to determine the transverse stress was obtained from previous equibiaxial flexural strength tests of similar ceramics performed in literature [12-14]. Using this test method allows for samples with reduced preparation induced defects, easier fabrication allowing for an increase in fracture tests (N≤30), specimens representative of LWR reactor fuel forms, reduced materials handling, and reduced material waste.

3. FABRICATION OF UO_2 AND DOPED UO_2

Nominally-pure UO_2 samples were fabricated of representative grain size and porosity as a method to benchmark results obtained here against literature data for UO_2. Dopants introduce a range of complexities including inhomogeneous distribution and possible secondary phases; prior to investigating their impacts, it was necessary to establish the validity of TRS to determine fracture strength of pure UO_2 compared to the literature. The methods used to date to prepare doped UO_2 samples are described below, but reporting on their impact on fracture properties is deferred to future investigations.

3.1 Fabrication of Doped UO_2

The doped UO_2 samples were prepared using a 99.8% purity UO_2 powder from International Bio-Analytical Industries, Inc. with an as received particle size of < 50 mesh (297 µm), as stated by the vendor. The powder reference density is 10.96 g/cm^3. The two dopants used for the fabrication of these doped samples, Cr_2O_3 and TiO_2 powders, were obtained from Alfa Aesar have a purity of 99.7% with particles sizes of <22 mesh (800 µm) and 15 nm, respectively, as stated by the vendor. As received UO_2 powder and 3000 wppm Cr_2O_3 and TiO_2 dopants were high energy planetary ball milled (HEPBM) in a zirconia vessel with a 10:1 media (YSZ media) to powder ratio for 12 hours at 500 rpm to reduce particle size and homogenize the powder. The as received UO_2 and dopant powders were reduced to submicron particles as seen in the SEM images in Figure 3**Error! Reference source not found.**. This allowed for better powder packing of the green pellets and higher surface area leading to increased sintered densities. Images of ball milled powder were not clear enough to resolve individual particle edges, but it is evident that particle sizes were reduced to submicron with some micron size agglomerates. The HEPBM UO_2 + dopant powder was mixed with 0.45 wt% Ethylene bis(stearamide) (EBS) binder for 1 hour at 150 rpm with YSZ media using a mixer mill.

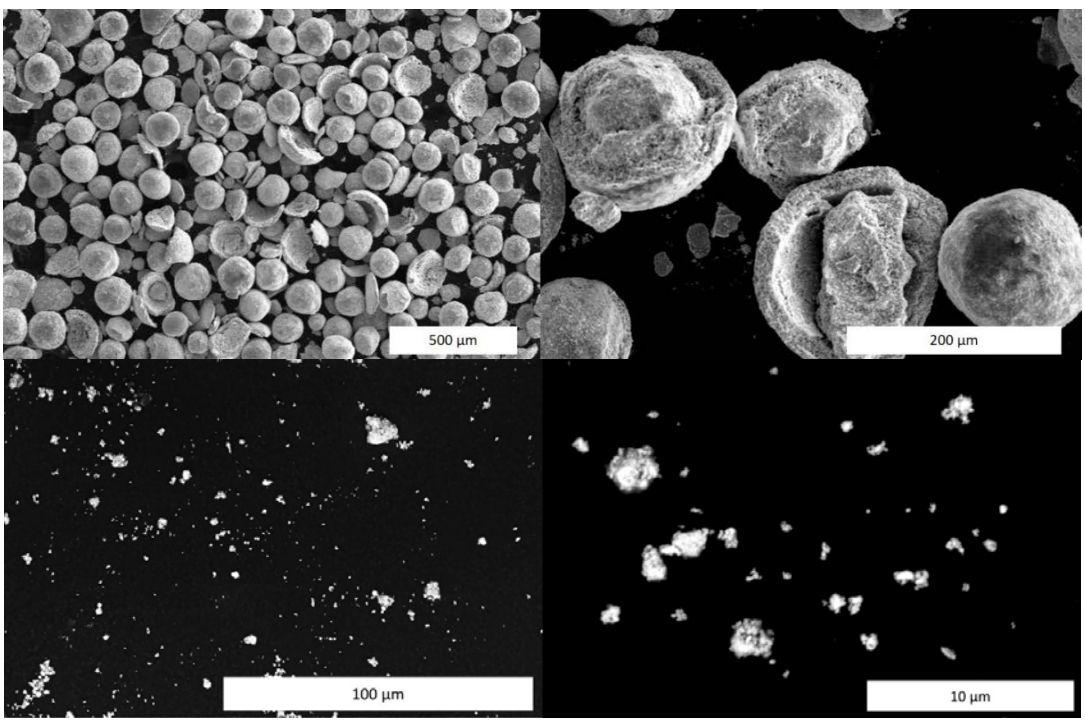

Figure 3. As received UO_2 powder (top images) and HEPBM doped UO_2 powder (bottom images) showing the drastic particle reduction during the HEPBM process used to integrate doping elements and create more surface area for increasing the sintered density.

Doped UO_2 samples were pressed into pellets using a dual action die at 150 MPa and held for 2 minutes. The pellets were placed in an alumina crucible with an alumina lid. Samples were sintered in an alumina tube furnace (CM Furnaces, Inc.). The sintering profiles and atmospheres (UHP Ar, UHP Ar+6% H_2, Ar+100ppm O_2) are represented in Figure 4 below [15-18]. The sintering conditions used in this study were selected based upon those available in the open literature. Prior to starting the sintering run, a vacuum-purge cycle was completed 3 times using the desired sintering gas and 10^{-3} Torr vacuum. The gas flow was maintained at a steady rate of 0.04 ml/min from the start to finish of each sintering run. All samples were sintered at a temperature of 1600 °C for 4 hours (Cr_2O_3 dopant) and 6 hours (TiO_2 dopant). A 2 hour binder burnout stage at 300 °C was used for all samples to ensure that the EBS binder was burnt out of the pellets prior to the sintering stage. Sintered pellets were imaged, Archimedes density was recorded, and pieces of each pellet were used for XRD, ICP-MS, and polished for SEM and EDS.

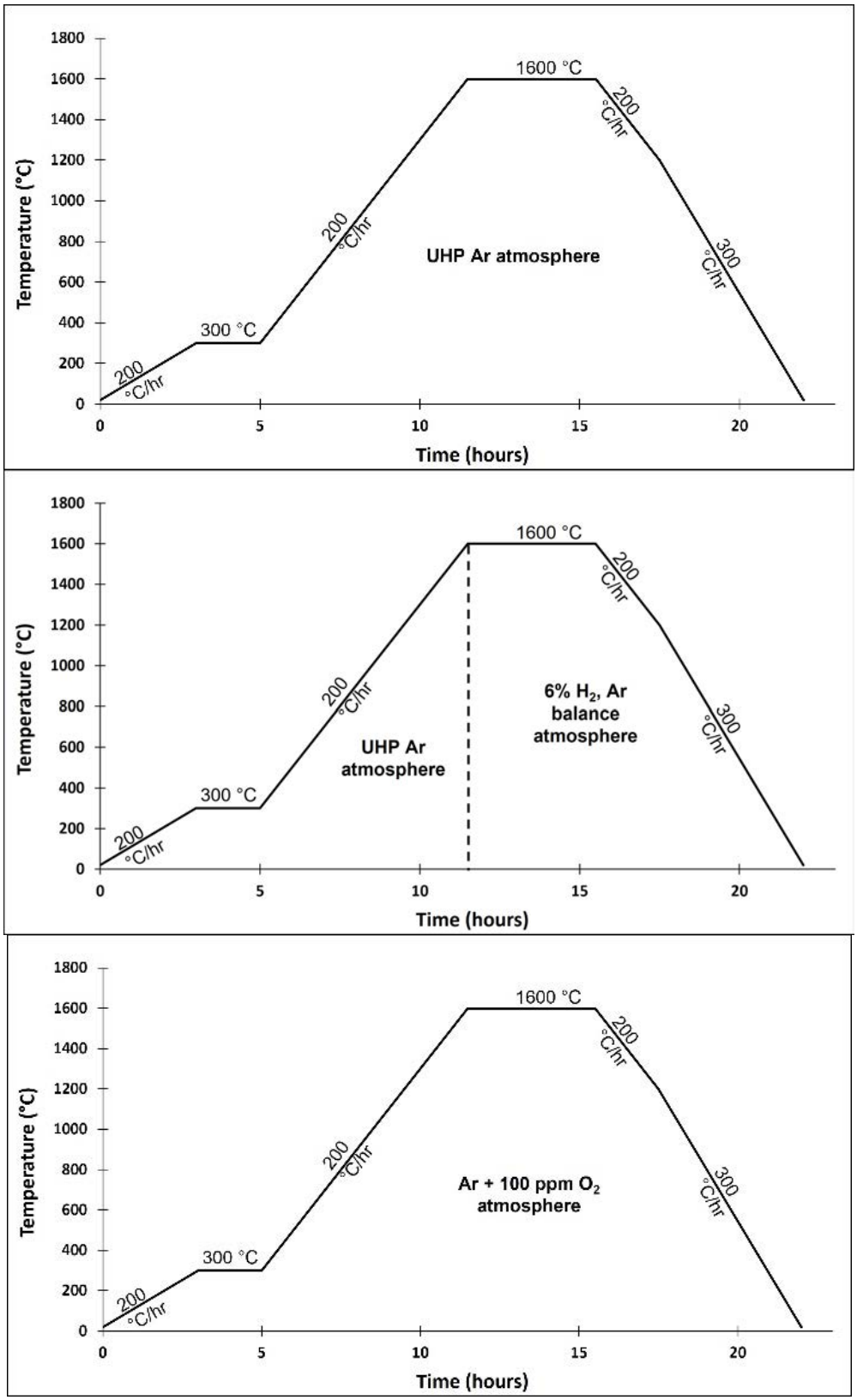

Figure 4. Sintering profiles and atmospheres for doped UO_2 sample fabrication. All samples were sintered at 1600 °C with a binder burnout stage at 300 °C.

3.2 Characterization of UO_2 and Doped UO_2

below lists the sintering conditions, Archimedes density measurements, and grain size data for pure UO_2 and each doped UO_2 sample sintered under the different atmospheres. Densities above 90% were obtained for pure UO_2 and most Cr_2O_3 pellets sintered in this work. The TiO_2-doped samples were all of low density. This result was unexpected as previous investigations have found good behavior in TiO_2-doped UO_2 at additions up to 4000 wppm [18]. Cursory characterization is performed of the TiO_2-doped samples, but additional work is necessary to understand the reason for the poor sintering behavior.

Table 1. Sintering conditions, Archimedes density and grain size analysis for Cr_2O_3 and TiO_2 doped UO_2 samples fabricated.

Sintering Atmosphere	Sintering Time (hrs)	Density (% TD)	Grain No. (dimensionless)	Grain Size (µm)
Pure UO_2 Pellet				
UHP Ar + 6% H_2	4	94 ± 0.5	11.5	5.6-6.7
3000 wppm Cr_2O_3-doped UO_2 Pellets				
UHP Ar	4	94 ± 0.5	5.4	53.4-63.5
UHP Ar + 6% H_2	4	91 ± 0.5	12.3	4.7-5.6
Ar + 100 ppm O_2	4	84 ± 0.5	13.2	3.3-4.0
3000 wppm TiO_2-doped UO_2 Pellets				
UHP Ar	6	74 ± 0.5	7.7	22.5-26.7
UHP Ar + 6% H_2	6	72 ± 0.5	8.9	15.9-18.9
Ar + 100 ppm O_2	6	73 ± 0.5	8.4	18.9-22.5

X-ray diffraction (XRD) was performed on as received, HEPBM and sintered powder to verify phase and purity pre- and post-processing. Energy dispersive spectroscopy (EDS) was used to investigate the chemical composition of the sintered doped UO_2 pellets. This analysis was performed to determine if any chemical impurities (i.e., Al, Y, Zr, etc.) or dopants (i.e., Cr_2O_3, TiO_2) were present in the sintered samples. Doped starting powder and sintered samples are being analyzed using inductively coupled plasma mass spectroscopy (ICP-MS). This analysis will confirm if the starting dopant concentration matches the target concentration and determine the levels of dopant remaining in the samples post sintering. The analysis has not been completed but results are expected with the next two to three weeks. The density of sintered samples was obtained using Archimedes density measurements with 22 °C DI water as the immersion fluid.

Powder XRD patterns are shown in Figure 5 for as received UO_2, HEPBM doped UO_2, and sintered doped UO_2 pellets (Cr_2O_3 or TiO_2) which were indexed using the ICSD database. Upon further examination of the as received UO_2 powder XRD pattern, it was noted there were several peaks which did not belong to the UO_2 profile. After magnifying the secondary peaks, it was determined there exists UO_3, U_3O_8, and an unidentified peak (seen at 35° 2Θ) in the as received material. The vendor's fabrication methods revealed that the starting U_3O_8 powder is converted to UO_3 prior to forming the UO_2. The vendor confirmed that a small fraction of UO_3 could be present in the sample due to fabrication methods. In addition, the U_3O_8 phase was likely formed as the UO_2 slowly oxidizes. After HEPBM the UO_2 the peaks broaden and the secondary peaks cannot be resolved. Post sintering it appears these secondary peaks are no longer present in the UO_2 sample.

After HEPBM the UO_2 the peaks broaden and the secondary peaks cannot be resolved. Post sintering, in all atmospheres, it appears these secondary peaks are no longer present in the pure or doped UO_2 samples. In the Cr_2O_3-doped UO_2 pellet sintered under ultra high purity (UHP) Ar, there were some unexpected

peaks present in the XRD pattern. After further examination it was determined these peaks correlate to tungsten oxide (WO_3) peaks. This is likely due to tungsten foil used in the fabrication of the pure UO_2 pellets. The WO_3 phase is observed in the XRD pattern for the first pellet fabricated (Cr_3O_2-doped UO_2 sintered under UHP Ar) but not seen in XRD patterns of subsequently sintered pellets (Figure 5). However, tungsten was also detected in the second pellet fabricated (Cr_2O_3-doped UO_2 sintered under UHP Ar + 6% H_2) using EDS as shown in the EDS map scan in Figure 8b. EDS did not detect tungsten in the Cr_2O_3-doped UO_2 pellet sintered under Ar + 100 ppm O_2 or in any of the TiO_2-doped UO_2 pellets.

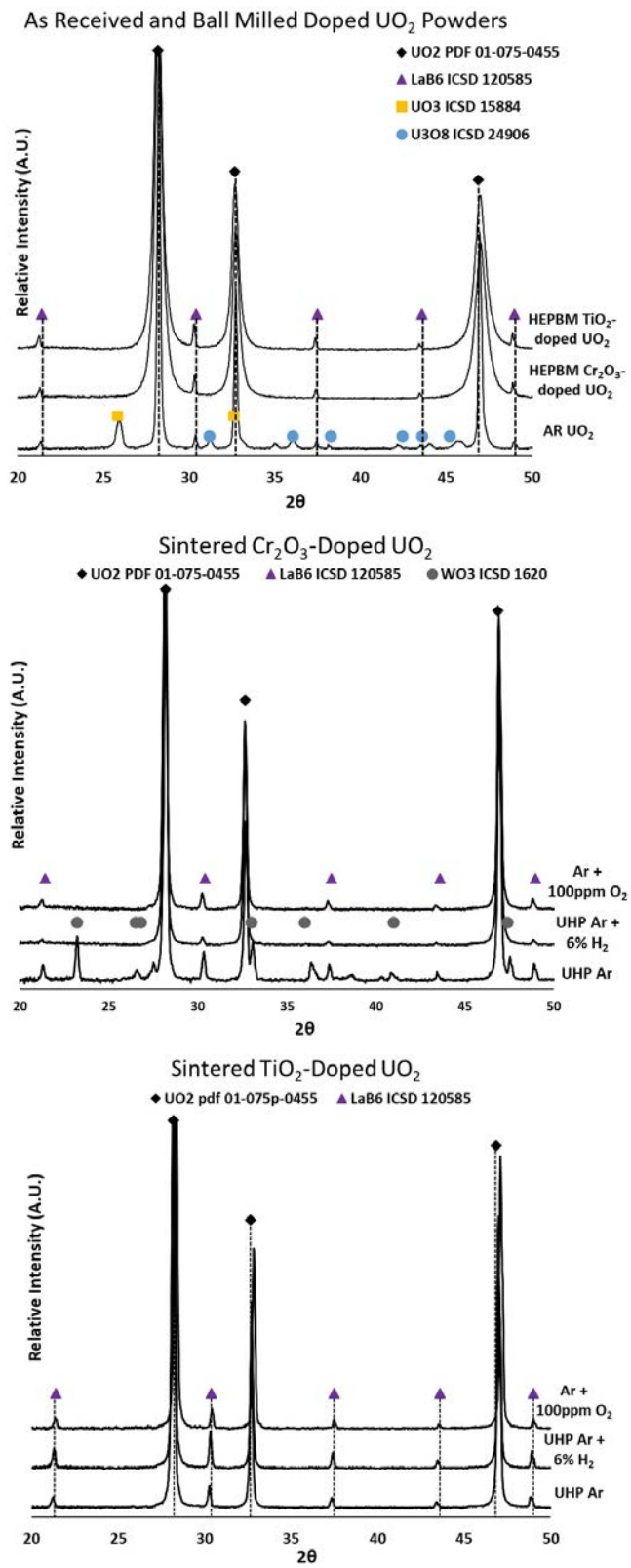

Figure 5. X-ray diffraction patterns for as received UO_2, ball milled doped UO_2 powders, and pellets sintered under different atmospheres doped with Cr_2O_3 and TiO_2 additives.

EDS maps were obtained for each doped sample sintered under the different atmospheres and thermally etched to reveal microstructure. The EDS data from the map scans is summarized in Table 2 below. Due to the low doping concentrations (0.3 wt%) and expected volatilization of the oxide additives during sintering, high accuracy and/or detection of dopants using EDS was not expected. EDS can detect minor concentrations (concentrations between 1 and 10 wt%) and has a detection limit of 0.1 wt% for bulk materials which is higher than the Cr_2O_3 and TiO_2 doping concentrations in this study [19]. However, although samples were doped below the theoretical detection limit, dopant elements (Cr^+ and Ti^+) were detected in the Cr_2O_3-doped UO_2 samples for each sintering atmosphere and in the TiO_2-doped UO_2 samples sintered under UHP Ar and Ar + 100 ppm O_2. This is likely due to the dopant cations precipitating into clusters throughout the samples which makes it easier for the EDS system to detect a Cr or Ti signal. Additionally, Zr was also observed in each of the sintered doped-samples. Fabrication of pure UO_2 pellets used 6 hour, 250 rpm milling parameters and no Zr was observed in the sintered samples, whereas the doped UO_2 samples were fabricated using 12 hours, 500 rpm milling parameters. This extended milling time appears to have caused a Zr contamination from the yttria-stabilized zirconia (YSZ) media and YSZ vessel used. Furthermore, some samples appear to also include Al and Si, which is likely due to the alumina crucible which typically contain Si and Na impurities. This will be investigated, along with the alumina sintering tube, prior to making additional samples.

Table 2. Energy dispersive spectroscopy data based on chemical maps for each sample.

Sintering Atmosphere	Dopant Cation (At%)	Other contaminants (At %)
3000 wppm Cr_2O_3-doped UO_2		
UHP Ar	1.4	0.3 Zr, 0.2 Al, 0.7 W
UHP Ar + 6% H_2	1.1	0.4 Zr, 0.3 Al, 0.5 W
Ar + 100 ppm O_2	1.2	0.5 Zr
3000 wppm TiO_2-doped UO_2		
UHP Ar	0.6	0.4 Zr, 0.3 Si
UHP Ar + 6% H_2	0	1.0 Zr, 0.3 Si
Ar + 100 ppm O_2	0.4	0.5 Zr, 0.4 Al, 04. Si

A grain size analysis was performed on thermally etched pure UO_2 pellets (shown in Figure 6) and doped UO_2 pellets (shown in Figures 5-10) using a circular intercept method according to ASTM standard E112-12. The average grain size number of the fabricated pure UO_2 was determined to be 11.5 which corresponds to an average grain size of 5.6-6.7 µm. From

we can see that the most drastic grain size increase was seen in the Cr_2O_3-doped UO_2 pellet sintered under UHP Ar for 4 hours. The grain size increased over 900% over the pure UO_2 with a doped UO_2 grain size range of 53.4-63.5 µm (Figure 7a). However, the EDS map in Figure 7b indicates that both W and Ti precipitated primarily along the grain boundaries. From XRD and EDS data it was evident the sample had a WO_3 phase present which could have played a role in the evolution of the microstructure. Accordingly, a new sample will be fabricated without the presence of tungsten to further investigate this in the next period of performance. The UHP Ar + 6% H_2 and Ar + 100 ppm O_2 sintering atmospheres produced Cr_2O_3-doped UO_2 pellets with lower densities and smaller grain sizes (Figure 8a and Figure 9a). All three sintering atmospheres produced poor theoretical densities (<75 % TD) for the TiO_2-doped UO_2 samples. The grain size did increase to the range of 15-25 µm (Figure 10, Figure 11, and Figure 12.

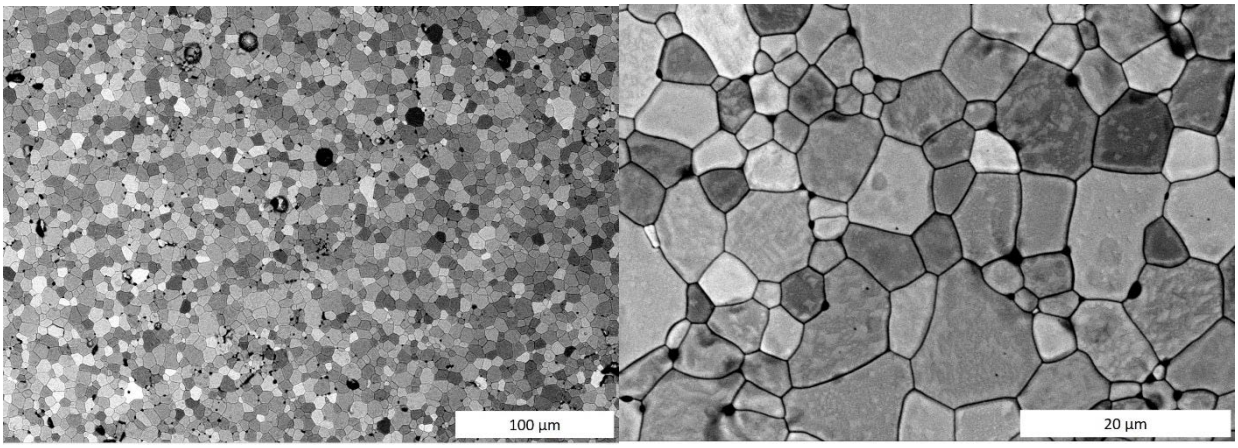

Figure 6. SEM images of thermally etched UO_2 pellet. Using ASTM standard E112-12, the average grain size number was determined to be 11.53 which corresponds to an average grain size of 5.6-6.7 µm with a TD of 94 ± 0.5 %.

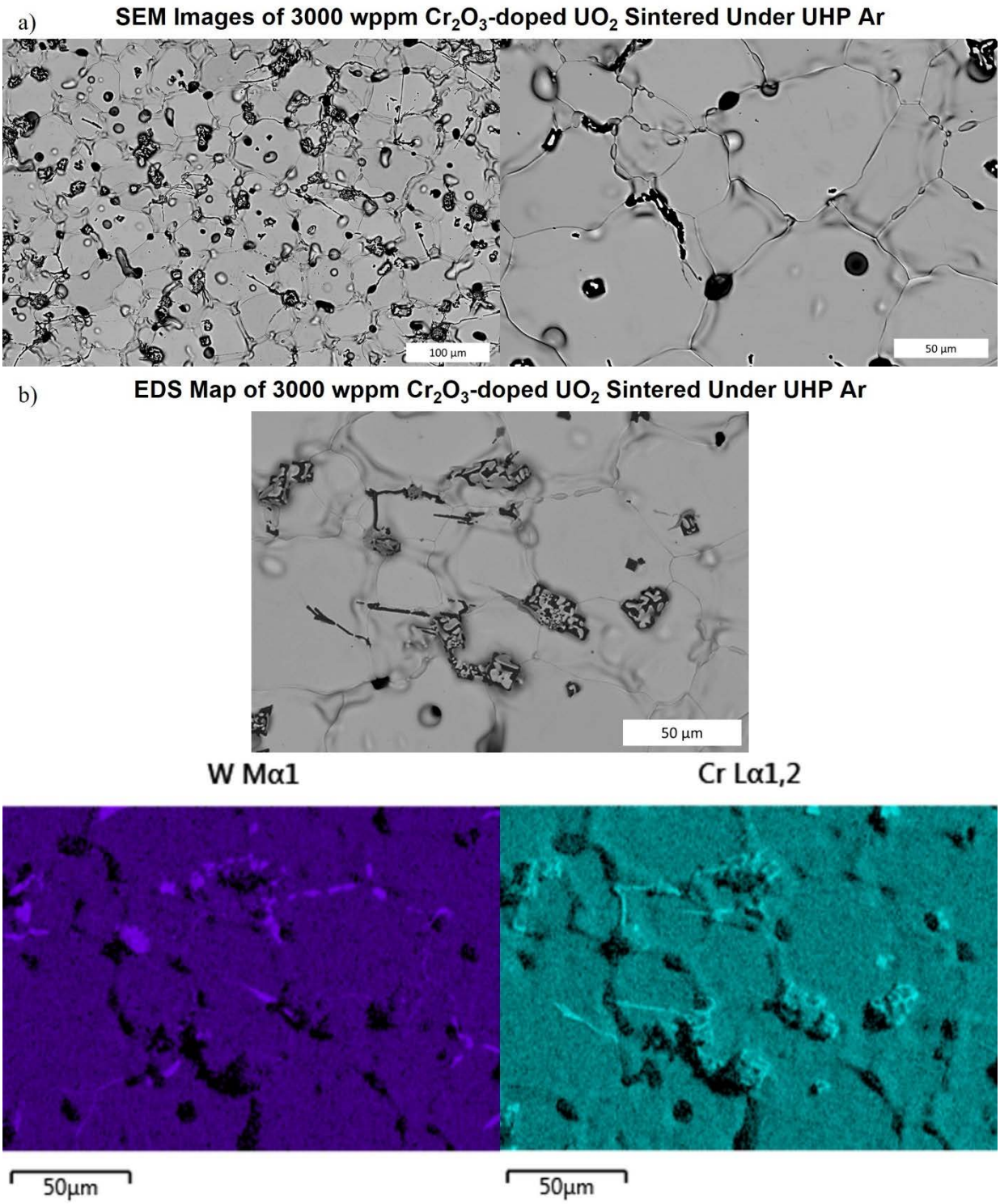

Figure 7. a) SEM images of thermally etched 3000 wppm Cr_2O_3-doped UO_2 pellet sintered under UHP Ar for four hours. The average grain size number was determined to be 5.4 with a grain size of 53.4-63.5 µm with a TD of 94 ± 0.5 %. b) EDS map scan detected the presence of W and Cr precipitated primarily along grain boundaries.

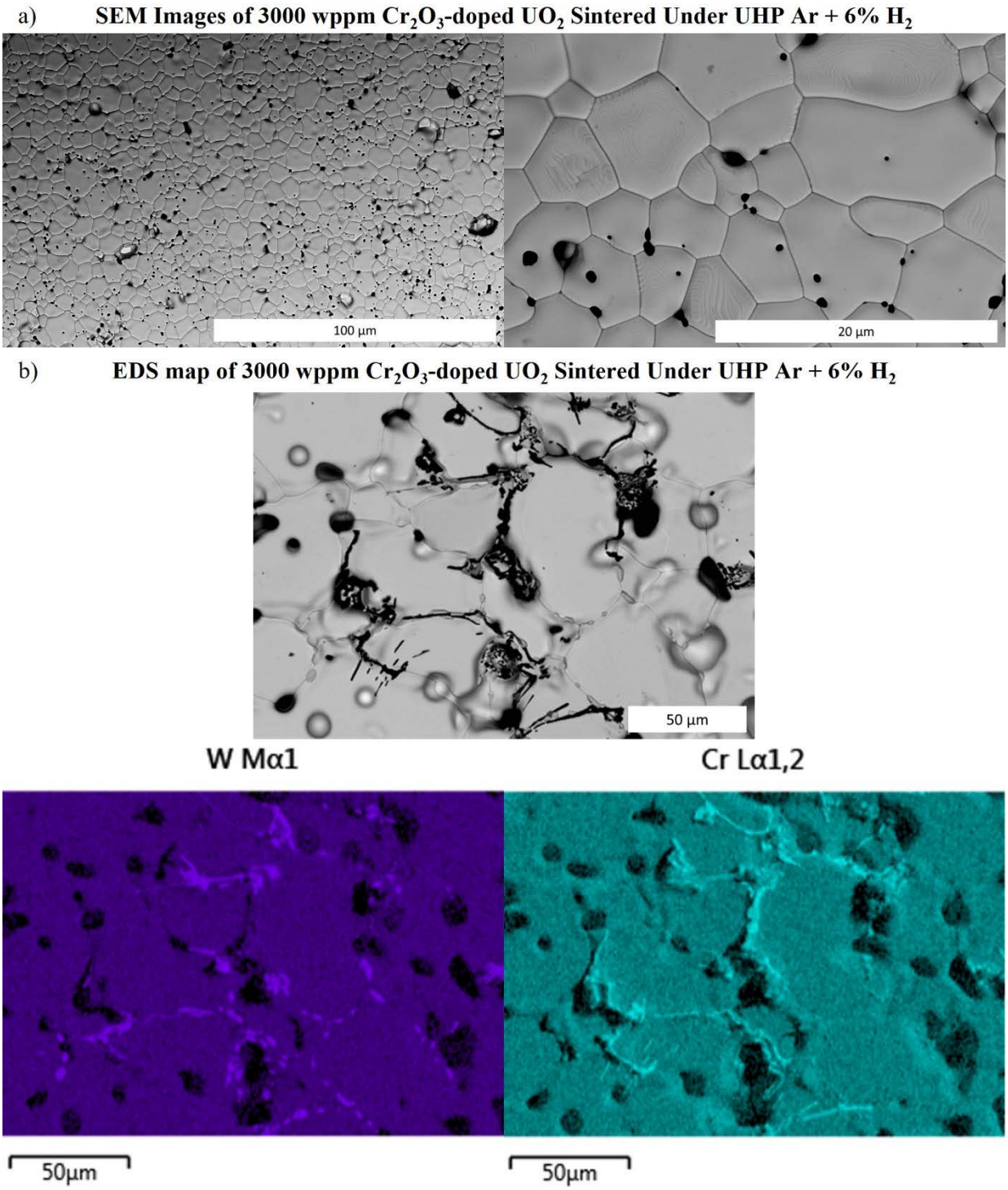

Figure 8. a) SEM images of thermally etched 3000 wppm Cr2O3-doped UO_2 pellet sintered under UHP Ar+6% H_2 for four hours. The average grain size number was determined to be 12.3 with a grain size of 4.7-5.6 µm with a TD of 91 ± 0.5 %. b) EDS map scan detected areas with the presence of W and Cr precipitated primarily along grain boundaries.

a) **SEM Images of 3000 wppm Cr_2O_3-doped UO_2 Sintered Under UHP Ar + 100 ppm O_2**

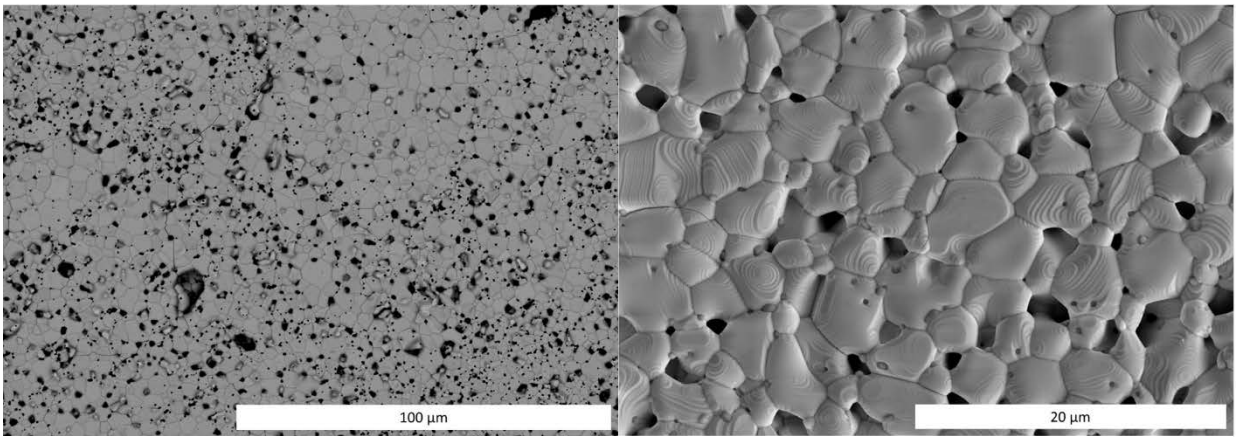

b) **EDS map of 3000 wppm Cr_2O_3-doped UO_2 Sintered Under UHP Ar + 100 ppmO_2**

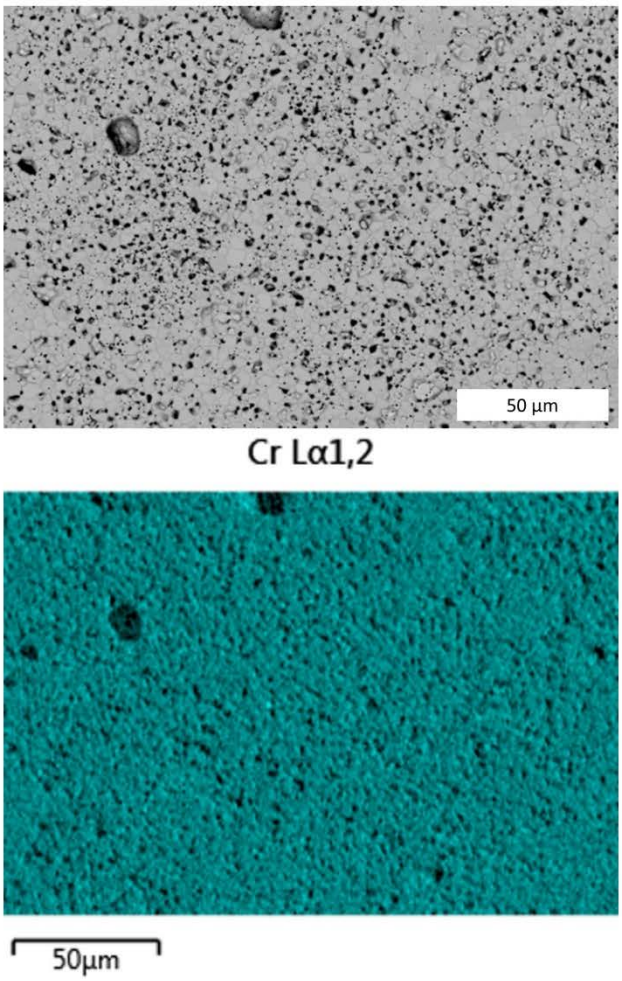

Figure 9. a) SEM images of thermally etched 3000 wppm Cr2O3-doped UO_2 pellet sintered under Ar+100 ppm O_2 for four hours. The average grain size number was determined to be 13.2 with a grain size of 3.3-4.0 µm with a TD of 84 ± 0.5 %. b) EDS map scan detected Cr which appears to be distributed primarily homogeneously throughout the sample.

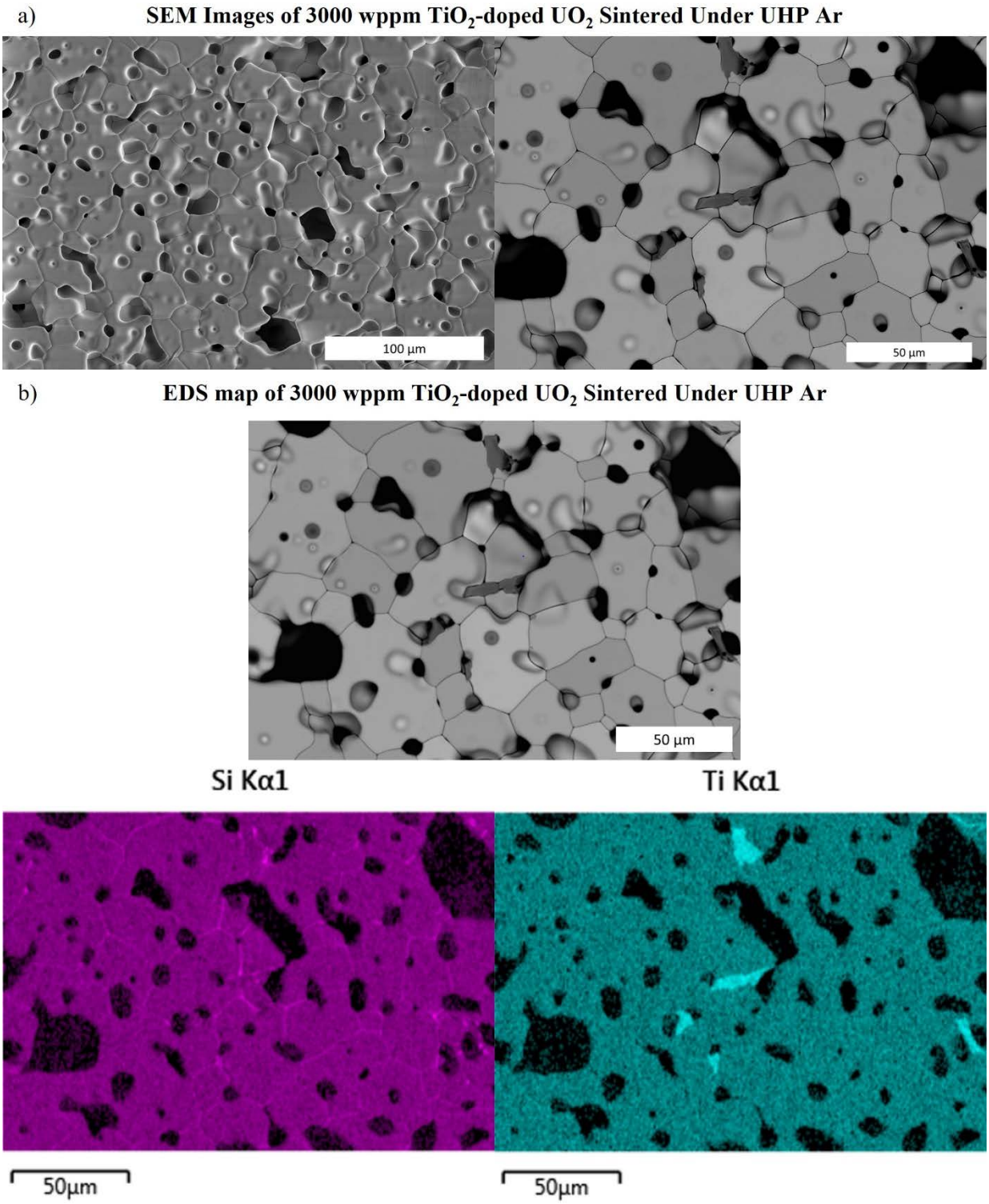

Figure 10. a) SEM images of thermally etched 3000 wppm TiO_2-doped UO_2 pellet sintered under UHP Ar for four hours. The average grain size number was determined to be 7.7 with a grain size of 22.5-26.7 µm with a TD of 74 ± 0.5 %. b) EDS map scan detected regions where Ti appears to have formed a eutectic liquid phase and Si deposited along grain boundaries.

a) SEM Images of 3000 wppm TiO_2-doped UO_2 Sintered Under UHP Ar + 6% H_2

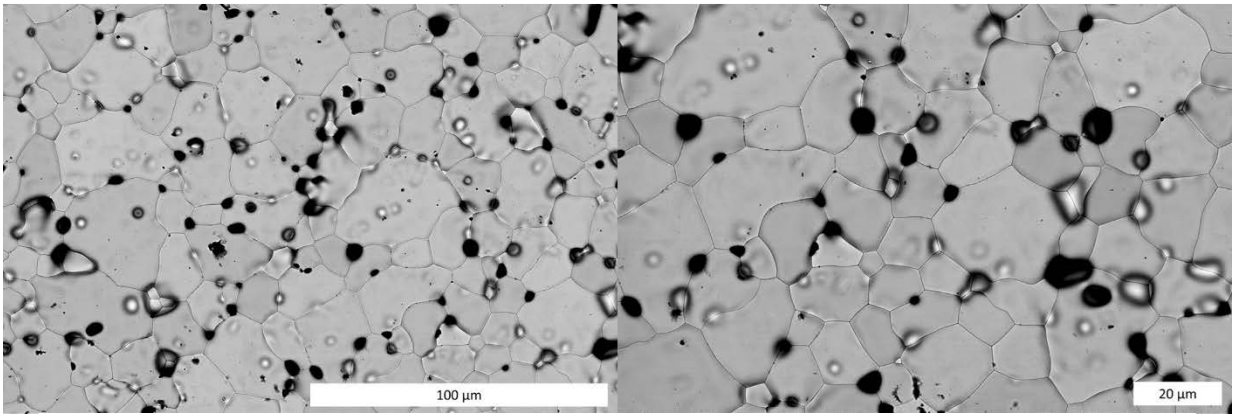

b) EDS map of 3000 wppm TiO_2-doped UO_2 Sintered Under UHP Ar + 6% H_2

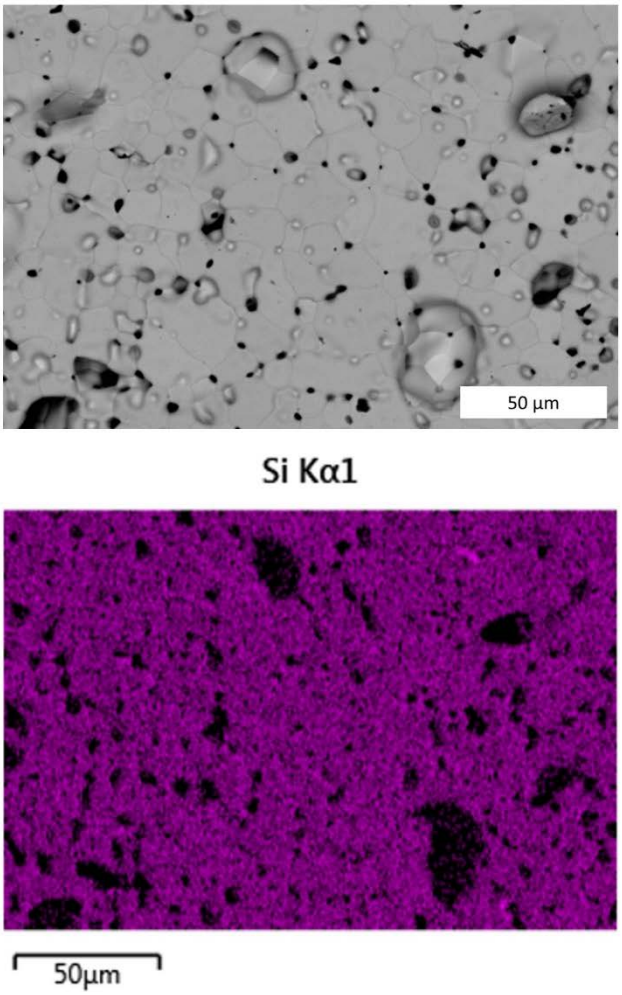

Figure 11. a) SEM images of thermally etched 3000 wppm TiO_2-doped UO_2 pellet sintered under UHP Ar+6 % H_2 for four hours. The average grain size number was determined to be 8.9 with a grain size of 15.9-18.9 µm with a TD of 72 ± 0.5 %. b) EDS map scan detected Si contaminants that appear to be primarily homogeneous throughout the sample. Ti was not detected in the sample.

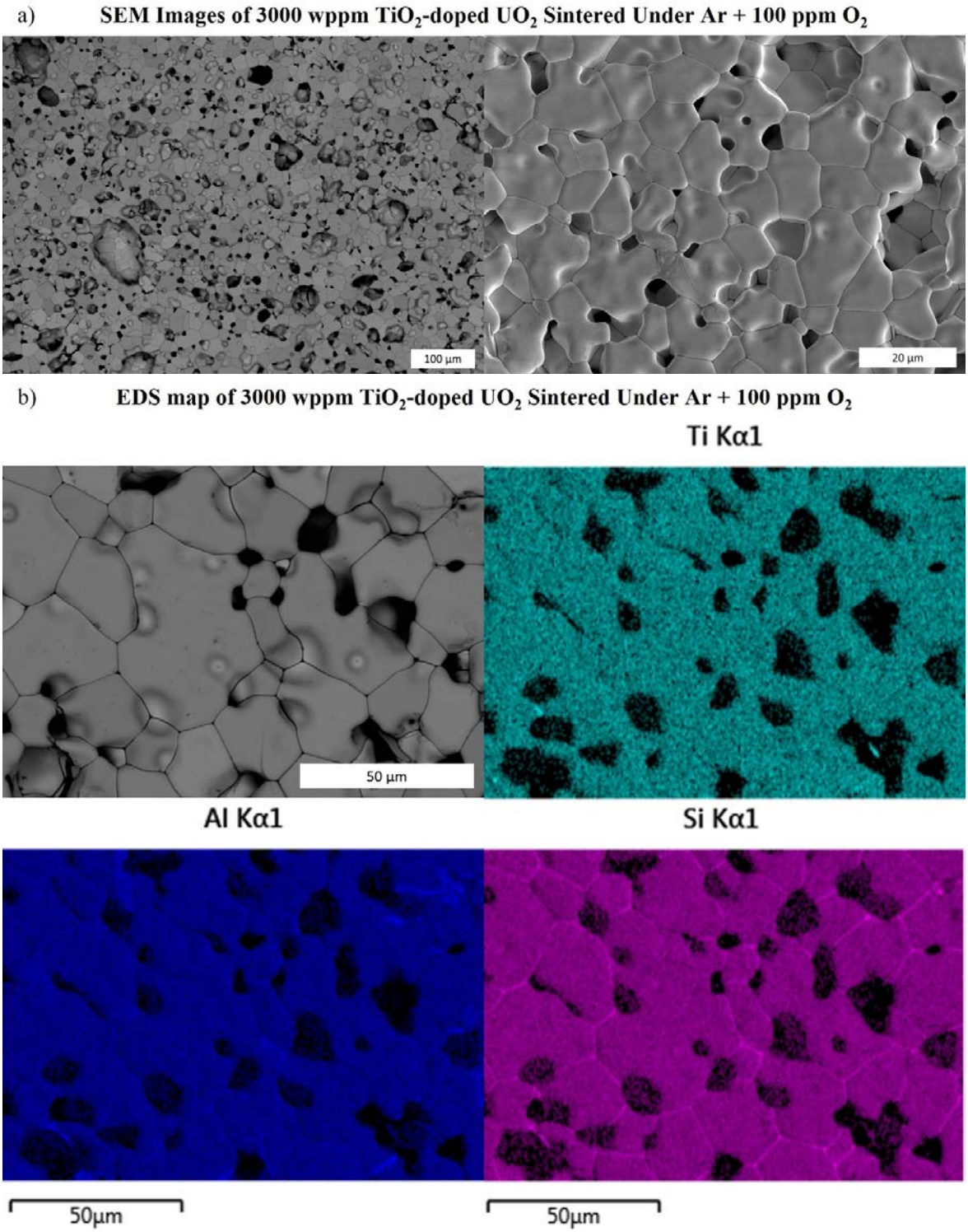

Figure 12. a) SEM images of thermally etched 3000 wppm TiO_2-doped UO_2 pellet sintered under UHP Ar+100 ppm O_2 for four hours. The average grain size number was determined to be 8.4 with a grain size of 18.9-22.5 µm with a TD of 73 ± 0.5 %. b) EDS map scan indicates there is some small cluster regions of Ti and Al as well as Si along grain boundaries in some regions of the sample. The Al and Si are likely due to crucible contamination.

4. RESULTS AND DISCUSSION

Nominal purity UO_2 specimens prepared as described above were tested at room temperature using TRS. The preliminary results of this testing and Weibull analysis are presented below. The TRS method was found to be capable of producing satisfactory fracture of the UO_2 disks prepared in this study.

4.1 Specimen Fracture

Table 3 lists the geometric and Archimedes density measurements and displays macro images of each UO_2 sample post TRS tests. Out of the 30 test samples, 17 samples fractured into three pieces while 13 samples fractured into two pieces.

Table 3. Geometric (G) and Archimedes (A) density of UO_2 samples using a reference density of 10.96 g/cm^3[20]. Images of fractured UO_2 pellets are included for each test specimen.

Test #	G Density (%TD)	A Density (%TD)	UO_2 Pellet Image (Post-test)	Test #	G Density (%TD)	A Density (%TD)	UO_2 Pellet Image (Post-test)
1	93±2%	94±2%	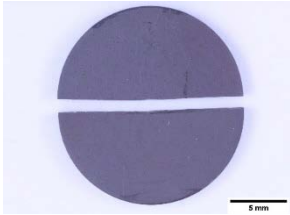	16	92±2%	94±2%	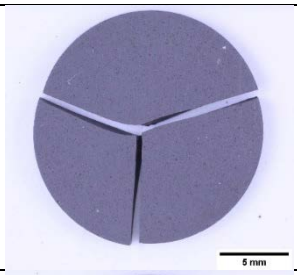
2	92±2%	94±2%	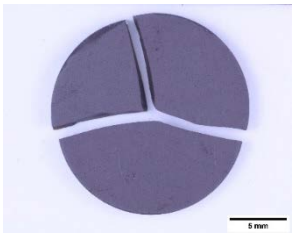	17	89±2%	94±2%	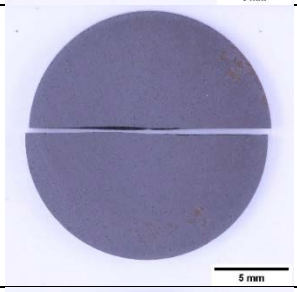
3	93±2%	95±2%	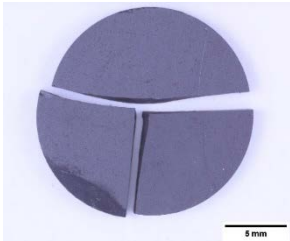	18	91±2%	94±2%	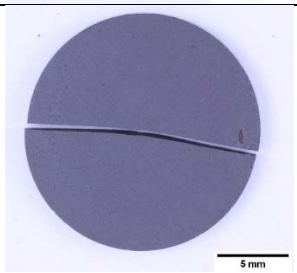

4	92±2%	95±2%	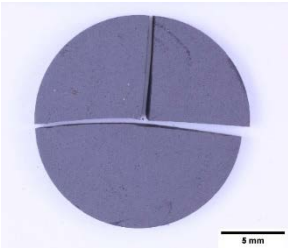	19	92±2%	94±2%	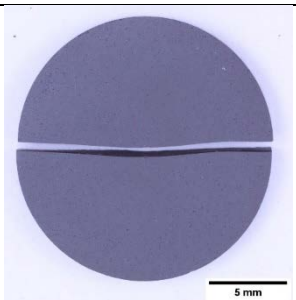
5	93±2%	95±2%	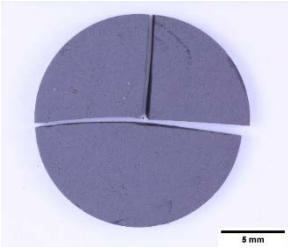	20	92±2%	95±2%	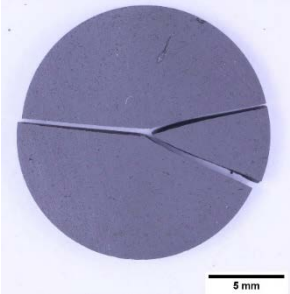
6	93±2%	94±2%	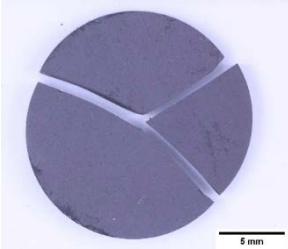	21	92±2%	94±2%	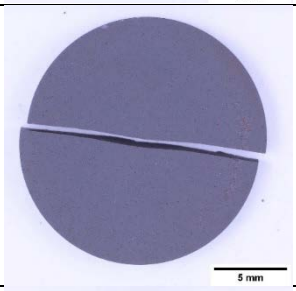
7	92±2%	94±2%	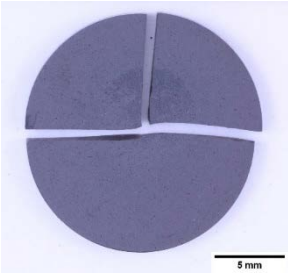	22	93±2%	94±2%	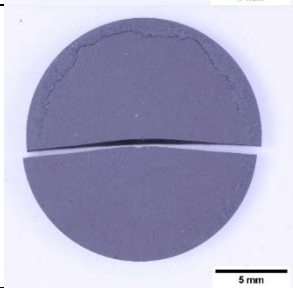
8	92±2%	95±2%	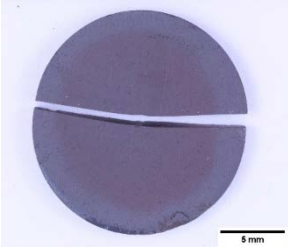	23	92±2%	94±2%	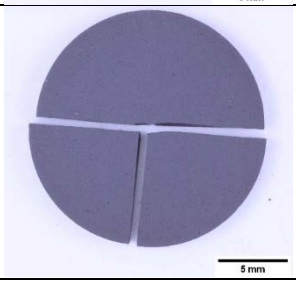

9	89±2%	94±2%	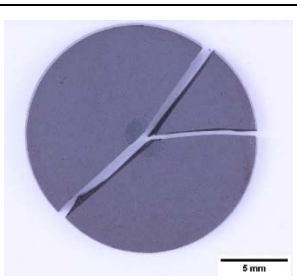	24	91±2%	94±2%	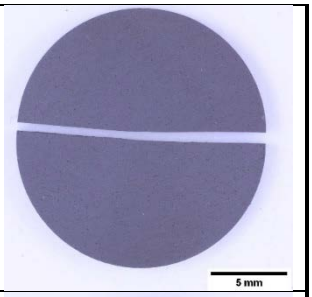
10	90±2%	94±2%	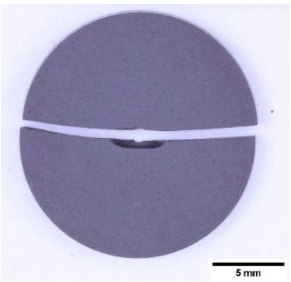	25	91±2%	94±2%	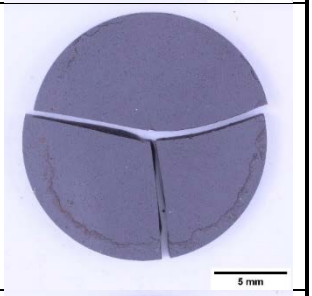
11	92±2%	94±2%	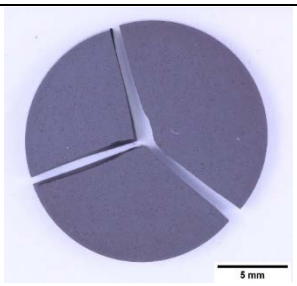	26	89±2%	94±2%	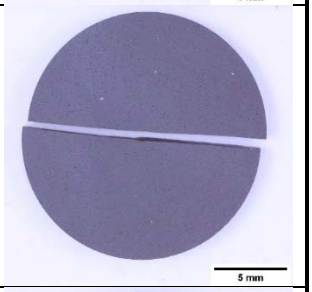
12	92±2%	94±2%	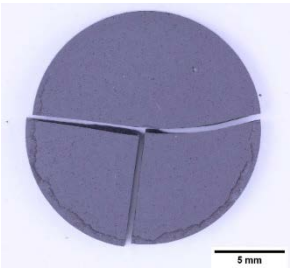	27	91±2%	94±2%	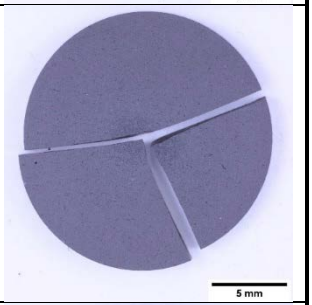
13	92±2%	94±2%	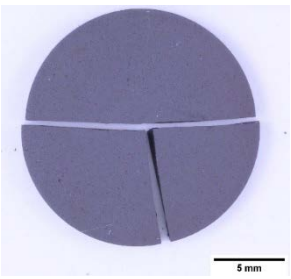	28	92±2%	94±2%	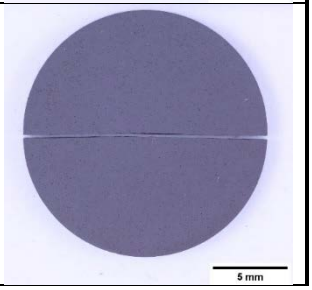

14	91±2%	94±2%	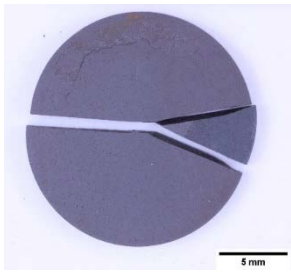	29	91±2%	94±2%	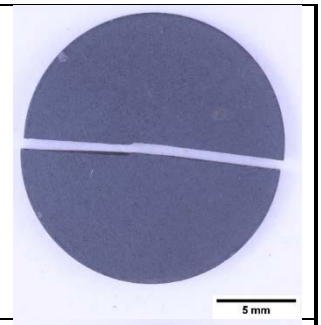
15	92±2%	94±2%	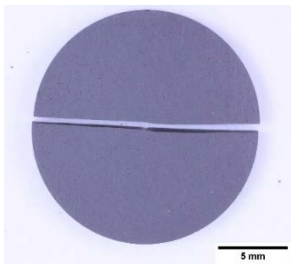	30	92±2%	94±2%	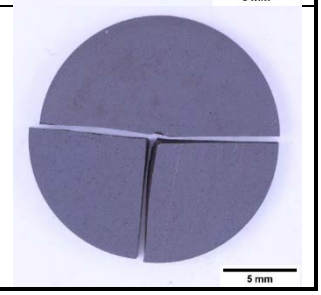

4.2 Transverse Rupture Strength Results

Force and displacement for each individual sample was collected using the MTS TestSuite Software and was converted to transverse stress using Equations 1-3, above, prior to plotting. Figure 13 shows the stress vs displacement curves for each test sample. To improve the clarity of the plots, transverse stress vs displacement values were only plotted to the maximum stress (transverse rupture stress). The initial noise in the load cell force reading (0.3-2.4 N) was removed from the max force which was then normalized to stress. All data exhibit the scatter expected of fracture in ceramics.

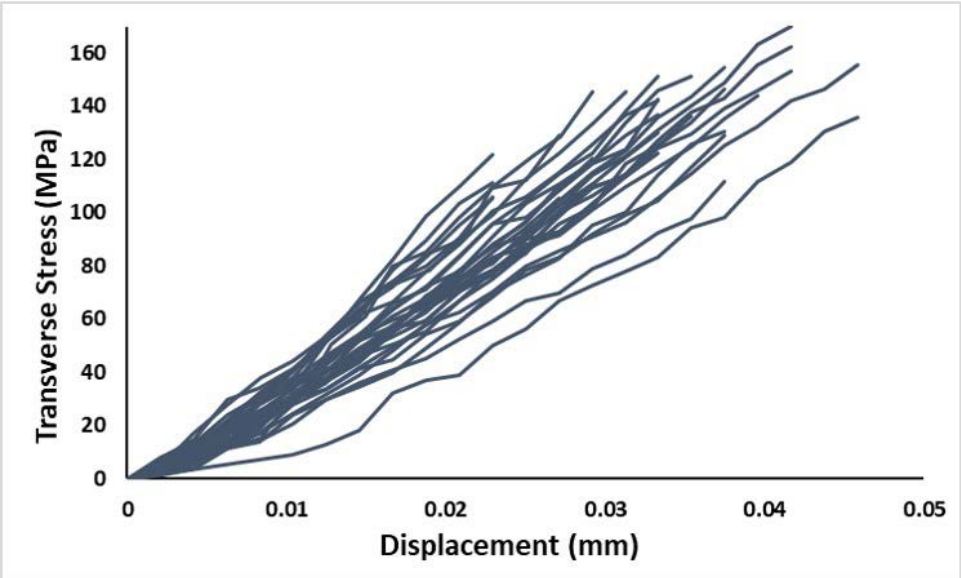

Figure 13. Transverse stress vs displacement curves for 30 UO_2 test specimens.

The maximum stress values recorded were documented as the transverse rupture strength for each sample. Table 4 summarizes the TRS data collected in this study. Fractured samples were imaged and stored in membrane cases for fracture analysis.

Table 4. Transverse stress values for UO_2 test specimens.

Test #	Transverse Stress (MPa)		Test #	Transverse Stress (MPa)		Test #	Transverse Stress (MPa)
1	145		11	130		21	148
2	147		12	134		22	148
3	122		13	134		23	149
4	130		14	135		24	155
5	112		15	137		25	156
6	145		16	139		26	157
7	146		17	142		27	158
8	147		18	145		28	160
9	123		19	146		29	166
10	127		20	147		30	171

Transverse rupture strengths observed in this study fall between 106 and 171 MPa. The technique used in this work was found capable of matching accepted literature values for both fracture strength and Weibull moduli, providing confidence in the method. However, mechanical properties will be a strong function of processing and microstructure. Nominally pure UO_2 as fabricated using a range of feedstocks, pressing conditions, and sintering profiles will be likely to yield a range of fracture behaviors.

Literature data focused on fracture of UO_2 is sparse. The MATPRO database on UO_2 properties provides a range of room temperature fracture data spanning 45 to 115 MPa [21]. However, surveys such as that performed by the compilers of the MATPRO compendium often simplify fracture strength to a single mean data point and omit the full range of fracture data collected. Assessment of the primary sources provides a broader range of data. Evans and Davidge report room temperature fracture spanning 140 to 182 MPa for UO_2 of similar density and grain size to this work [22]. A major limitation of many methods cited in the literature is that many investigators rely upon correlations rather than bulk measurements; for example, correlation of crack length as resulting from microindentation testing is a common approach [23]. These approaches have the advantage of being feasible in hot cell environments but cannot capture the statistical nature of fracture in ceramic materials.

4.3 Weibull Statistics Analysis

Due to the brittle and stochastic fracture of UO_2, a statistical analysis was performed on the TRS data obtained for 30 test specimens. The Weibull distribution of the probability of failure was used to describe the fracture behavior and obtain Weibull parameters. The classical relationship for the probability of failure (P_f) using Weibull statistics as shown in Equation 4,

$$\ln \ln \left(\frac{1}{1-P_f}\right) = m * ln\,[\frac{\sigma_f}{\sigma_0}] \tag{4}$$

where σ_f is the fracture strength, σ_0 is the characteristic strength, and m is the Weibull modulus. The Weibull parameters σ_0 and m can then be determined by plotting the equation in the form of a line, $y = m * x + b$. The characteristic strength is defined as the stress value at which 63.2% of all samples fail and the Weibull modulus provides information about fracture data scatter of the samples. The larger the Weibull modulus the less variation in fracture stress and the higher the degree of homogeneity between samples.

The Weibull parameters were calculated using Equation 4 and a linear fit to the data (Figure 14) where the slope of the line is the Weibull modulus. In addition, the characteristic strength was extracted at the point when the probability of failure (P_f) is equal to 63.2%, as seen in Figure 15. Table 5 summarizes TRS results and Weibull parameters the UO_2 test specimens.

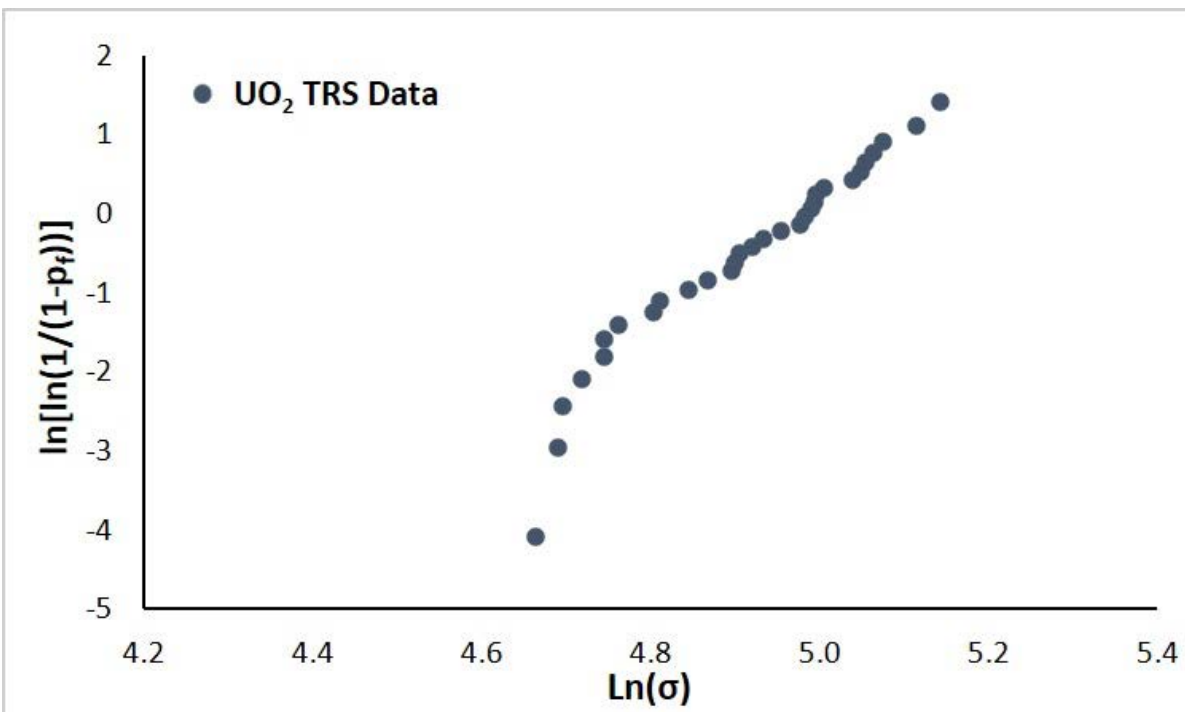

Figure 14. Weibull distribution plot for UO_2 test specimens (N=30). The Weibull modulus was recorded as 8.9 (dimensionless).

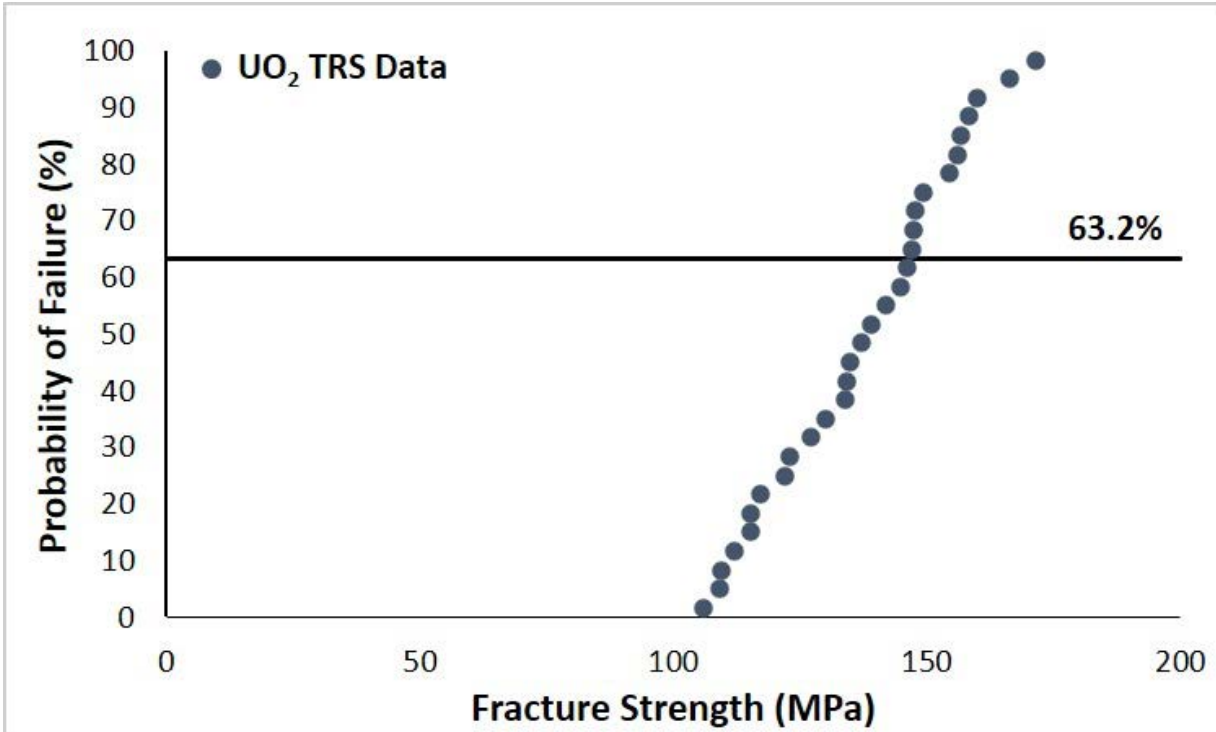

Figure 15. Probability of failure plot indicates the characteristic strength for UO_2 is approximately 146 MPa. This indicates that 63.2% of samples will not fracture below this stress threshold.

Table 5. TRS results and Weibull parameters for UO_2 test specimens.

TRS Range (MPa)	Average TRS (MPa)	Characteristic Strength [σ_0] (MPa)	Weibull Modulus [m]	Linear Fit [R^2]	No. Test Samples
106-171	138	146	8.9	0.94	30

4.4 Fracture Surface Characterization

Fracture surface for several pellets were imaged using a SEM. The fracture surface images shown in Figure 16 indicate that the fracture mode for the UO_2 samples is a mixture of intergranular and transgranular. Grain size seems to play a role in the fracture mechanisms observed where larger grains tend to have a transgranular fracture mode and smaller grains tend to have an intergranular fracture mode. Although the average grain size was estimated to be 6.7 µm a range of grain sizes was observed as shown in Figure 6. The range in grain sizes can also be observed in the fracture surface images below in Figure 16. Additionally, regions were observed where densification and grain growth were largely inhomogeneous as shown in image c) of Figure 16. The observation of porosity as highlighted in Figure 16c was the exception; the majority of the fracture surface of Sample 20 was found similar to Figure 16a and Figure 16b. Table 4 shows that the rupture strength of Sample 20 was near the median of all samples tested.

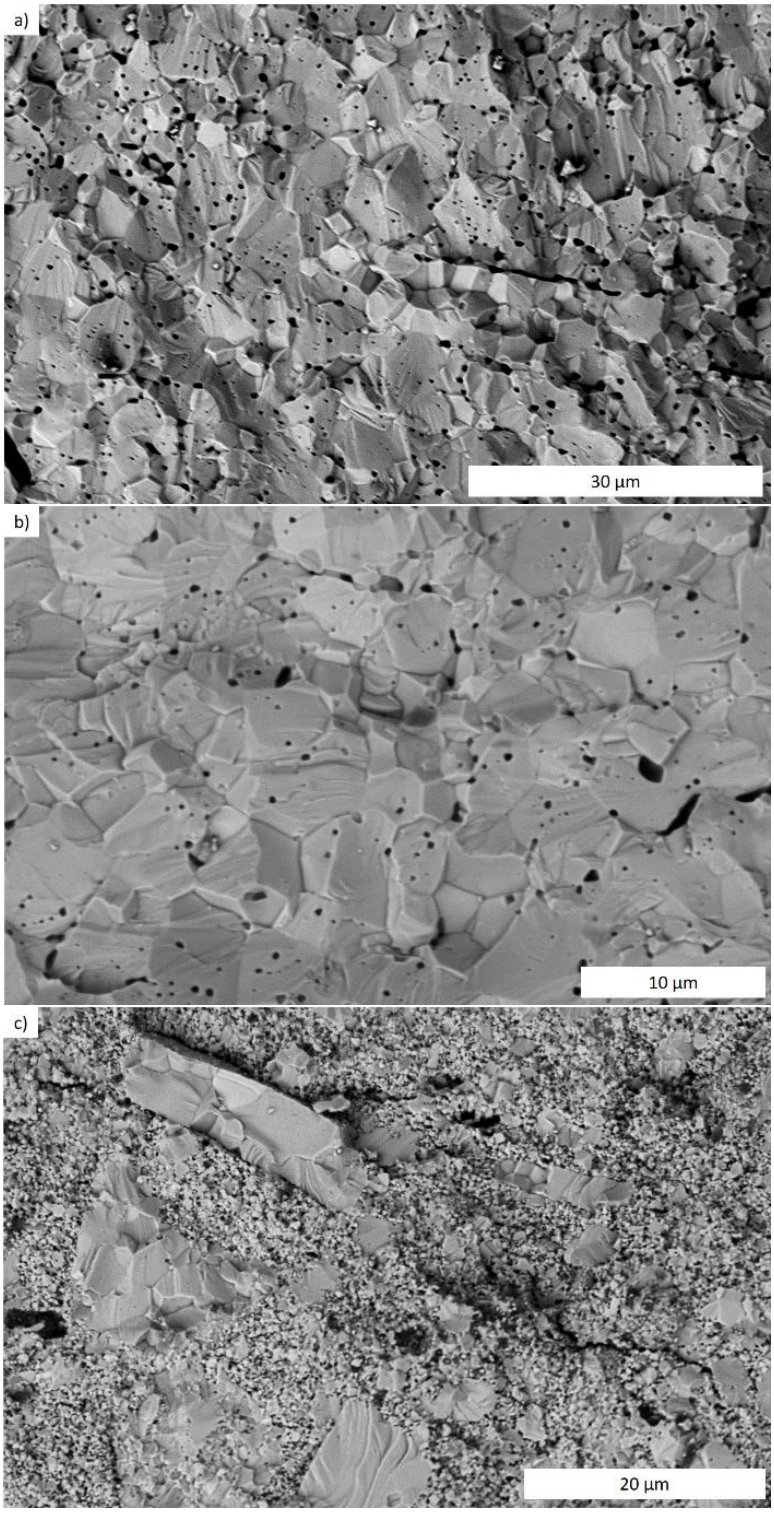

Figure 16. Fracture surface images of TRS tested UO_2 pellets indicate there is mixture of intergranular and transgranular fracture modes. a) sample 2, b) sample 12, and c) sample 20. The fracture surface shown in c) indicates noticeable porosity.

5. CONCLUSIONS

This report summarizes progress made in the characterization of fracture behavior in UO_2 using TRS. Fracture strength data for pure UO_2 is presented here for the first time. Data collected using this method is in general agreement with the limited literature data. Doped UO_2 samples were also synthesized to provide baseline material for additional TRS testing.

6. ACKNOWLEDGMENTS

The authors would like to acknowledge Rachel Seibert for review of the report and technical comments.

7. REFERENCES

[1] I.J. Hastings, A.D. Smith, P.J. Fehrenbach, T.J. Carter, Fission gas release from power-ramped UO 2 fuel, Journal of Nuclear Materials 139(2) (1986) 106-112.

[2] K. Une, K. Nogita, S. Kashibe, M. Imamura, Microstructural change and its influence on fission gas release in high burnup UO2 fuel, Journal of Nuclear Materials 188 (1992) 65-72.

[3] T. Zhang, R. Yue, X. Wang, Z. Hao, Failure probability analysis and design comparison of multi-layered SiC-based fuel cladding in PWRs, Nuclear Engineering and Design 330 (2018) 463-479.

[4] Y. Sumi, L.M. Keer, S. Nemat-Nasser, Thermally induced radial cracking in fuel element pellets, Journal of Nuclear Materials 96(1) (1981) 147-159.

[5] C. Bernaudat, Mechanical behaviour modelling of fractured nuclear fuel pellets, Nuclear Engineering and Design 156(3) (1995) 373-381.

[6] J.M. Gatt, J. Sercombe, I. Aubrun, A.C. Menard, Experimental and Numerical Study of Fracture Mechanisms in UO2 Nuclear Fuel Forms, Engineering Failure Analysis 47 (2015) 299-311.

[7] Y. Zhang, P.C. Millett, M.R. Tonks, X.-M. Bai, S.B. Biner, Molecular dynamics simulations of intergranular fracture in UO2 with nine empirical interatomic potentials, Journal of Nuclear Materials 452(1) (2014) 296-303.

[8] A. Nelson, S. Finkeldei, S. Dillon, B. Heuser, K. Terrani, Development of small-scale mechanical property measurement methods for irradiated fuel samples, ORNL/SPR-2019 (2019).

[9] A. Nelson, C. Silva, A. Lupercio, E. Moshkelgosha, R. Winters, C. Doyle, M. Mamivand, S. Dillon, B. Heuser, B. Jaques, Fracture Strength Determination Methods for Ceramic Materials Applied to Uranium Dioxide, ORNL/SPR-2020 (2020).

[10] A. Lupercio, E. Moshkelgosha, R. Winters, C. Doyle, M. Mamivand, A. Nelson, B. Jaques, Ball-on-ring Test Validation for Equibiaxial Flexural Strength Testing of Engineered Ceramics, International Journal of Ceramic Engineering & Science 3 (2021).

[11] B. Al-Makramani, A. Razak, M. Abu-Hassan, Biaxial Flexural Strength of Turkom-Cera Core Compared to Two Other All-Ceramic Systems, Journal of Applied Oral Science 18(6) (2009) 607-612.

[12] J. Eichler, J. Rodel, U. Eisele, M. Hoffman, Effect of Grain Size on Mechanical Properties of Submricometer 3Y-TZP: Fracture Strength and Hydrothermal Degradation, Journal of American Ceramic Society 90(9) (2007) 2830-2836.

[13] S. Ban, K.J. Anusavice, Influence of test Method on Failure Stress of brittle Dental Materials, Journal of Dental Research 69(12) (1990) 1791-1799.

[14] S. Poolthong, T. Mori, M. Swain, A comparison of the Mechanical Properties of Three Glass_ionemer Cements, Dental Materials 13(2) (1994) 220-227.

[15] B.J. Dooies, Enhancement of Uranium Dioxide Thermal and Mechanical Properties by Oxide Dopants, University of Florida Thesis (2008).

[16] S.C. Finkeldei, R.D. Hunt, J.O. Kiggans, C.A. Hobbs, B.D. Eckhart, Documentation Package Supporting the Fabrication of Doped UO2 Samples for MiniFuel Irradiation and Fission Gas Release Benchmarking, Oak Ridge National Laboratory (2019).

[17] R. Leckie, Evolutionary Enhancements to UO2, Los Alamos National Laboratory (2013).

[18] C. Silva, R. Hunt, A. Nelson, Microstructural and Crystallographic Effects of Sol-Gel Synthesized Ti-Doped UO2 Under Reducing Conditions, Journal of Nuclear Materials 552 (2021).

[19] SeifollahNasrazadani, ShokrollahHassani, Chapter 2 - Modern analytical techniques in failure analysis of aerospace, chemical, and oil and gas industries, Handbook of Materials Failure Analysis with Case Studies from the Oil and Gas Industry (2016) 39-54.

[20] S.G. Popov, J.J. Carbajo, V.K. Ivanov, G.L. Yoder, Thermophysical Properties of MOX and UO2 Fuels Including the Effects of Irradiation, Oak Ridge National Laboratory (2000).

[21] S.R.-D.C.D. Team, SCDAP/RELAP5-3D Code Manual Volume 4: MATPRO - A Library of Materials Properties for Light-Water-Reactor Accident Analysis, Idaho National Engineering and Environmental Laboratory (2003).

[22] A.G. Evans, R.W. Davidge, A. G. Evans and R. W. Davidge, "The strength and fracture of stoichiometric polycrystalline UO2, Journal of Nuclear Materials 33(3) (1969) 249-260.

[23] K. Kapoor, A. Ahmad, A. Laksminarayana, G.V.S. Hemanth Rao, Fracture properties of sintered UO2 ceramic pellets with duplex microstructure, Journal of Nuclear Materials 366(1) (2007) 87-98.